

Well-Defined Cobalt Catalyst with N-Doped Carbon Layers Enwrapping: The Correlation between Surface Atomic Structure and Electrocatalytic Property

Youkui Zhang, Yunxiang Lin, Hongliang Jiang,* Chuanqiang Wu, Hengjie Liu, Changda Wang, Shuangming Chen, Tao Duan, and Li Song*

Admittedly, the surface atomic structure of heterogenous catalysts toward the electrochemical oxygen reduction reaction (ORR) are accepted as the important features that can tune catalytic activity and even catalytic pathway. Herein, a surface engineering strategy to controllably synthesize a carbon-layer-wrapped cobalt-catalyst from 2D cobalt-based metal–organic frameworks is elaborately demonstrated. Combined with synchrotron radiation X-ray photoelectron spectroscopy, the soft X-ray absorption near-edge structure results confirmed that rich covalent interfacial Co–N–C bonds are efficiently formed between cobalt nanoparticles and wrapped carbon-layers during the polydopamine-assisted pyrolysis process. The X-ray absorption fine structure and corresponding extended X-ray absorption fine structure spectra further reveal that the wrapped cobalt with Co–N coordinations shows distinct surface distortion and atomic environmental change of Co-based active sites. In contrast to the control sample without coating layers, the 800 °C-annealed cobalt catalyst with N-doped carbon layers enwrapping achieves significantly enhanced ORR activity with onset and half-wave potentials of 0.923 and 0.816 V (vs reversible hydrogen electrode), highlighting the important correlation between surface atomic structure and catalytic property.

For heterogenous catalysis reaction, the surface atomic structure of heterogenous catalyst significantly influences catalytic behavior and even catalytic pathway.^[1–4] In particular, for electrochemical oxygen reduction reaction (ORR), robust yet low-cost catalyst is generally obtained via precise surface structure and component design.^[5–8] Recent works indicate that highly

oriented metal–organic frameworks (MOFs) or their composites can serve as important sacrificial precursors toward the synthesis of carbonaceous materials with well-defined surface atomic structure via a facile pyrolysis process.^[9–13] For example, MOFs derived hybrid materials with transition metals (e.g., Fe, Co, Ni) based heteroatoms (e.g., B, N, S)-doped carbon materials (e.g., carbon nanotubes, graphene) were believed to be promising candidates as electrocatalysts to substitute the Pt-based catalysts toward ORR, in acidic or alkaline media, owing to their low cost and desirable electrocatalytic activities.^[14–20] Among them, nitrogen and transition metals modified carbonaceous catalysts (denoted as M–N–C) have been shown to generate M–N_x moieties, which has been reported as highly effective catalytic active sites.^[17,21–23] Besides, the embedded transition metal nanoparticles can improve the electron transport and thereby enhance ORR activity,^[24–26]

and the nitrogen atom in carbon network can induce charge polarization to boost ORR activity.^[27,28] However, MOFs are often prone to structure collapse during the pyrolysis process, thus making further growth of metal particles into an uncontrollable bulk phase, which largely reduces the electrochemical performance.^[29–31] Therefore, it is highly desirable that the surface functionalization of MOFs via surface engineering realizes the integration of active components.^[32] However, it is still limited for the study and use of the MOFs precursor for the preparation of highly active M–N–C electrocatalyst for the ORR application.

Meanwhile, further identification of electronic and atomic structure toward these catalysts is also important to guide catalysts development for ORR. Recently, synchrotron radiation light-based spectroscopy technologies, such as X-ray spectroscopy techniques including synchrotron radiation X-ray photoelectron spectroscopy (SRXPS) and X-ray absorption spectroscopy (XAS) are generally introduced to investigate the atomic structures of catalysts.^[33] Especially, extensive interests have been devoted to utilization of XAS in analyzing atomic and electronic structures of photo/electrochemical catalysts,

Y. Zhang, Y. Lin, Dr. H. Jiang, C. Wu, H. Liu, C. Wang, Dr. S. Chen, Prof. L. Song

National Synchrotron Radiation Laboratory
CAS Center for Excellence in Nanoscience
University of Science and Technology of China
Hefei, Anhui 230029, China

E-mail: jhlworld@ustc.edu.cn; song2012@ustc.edu.cn

Y. Zhang, Prof. T. Duan

School of National Defense Science and Technology
Southwest University of Science and Technology
Mianyang, Sichuan 621010, China

 The ORCID identification number(s) for the author(s) of this article can be found under <https://doi.org/10.1002/sml.201702074>.

DOI: 10.1002/sml.201702074

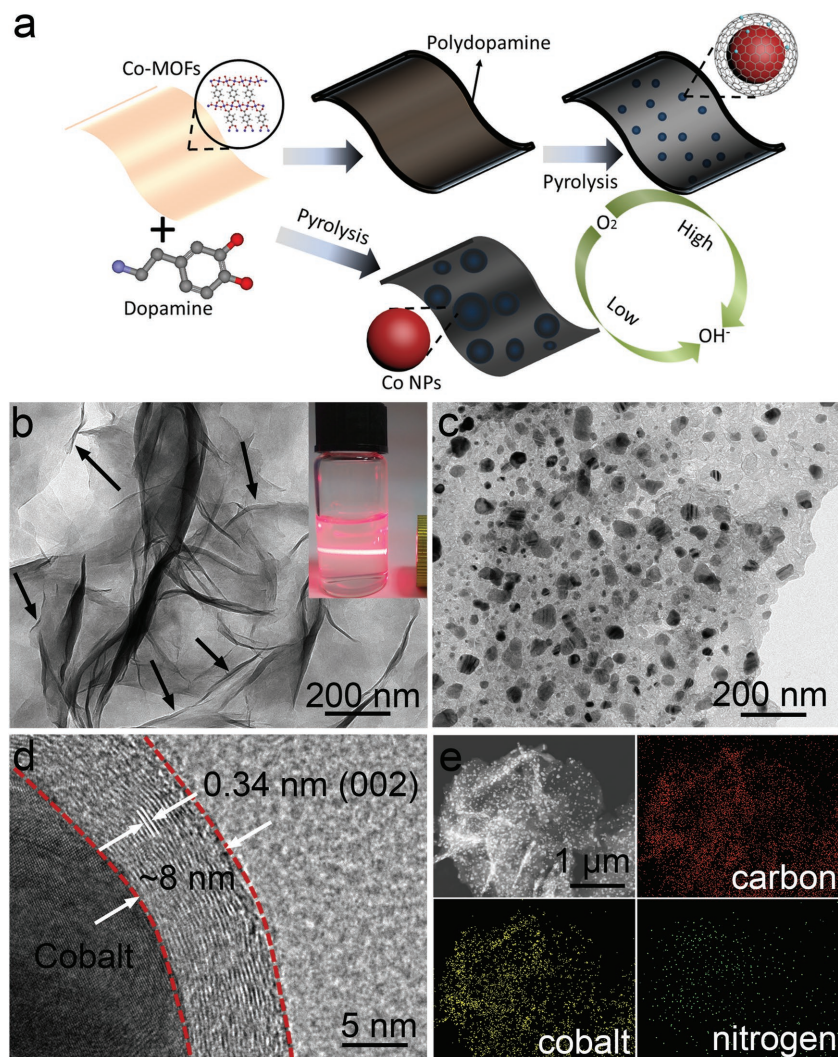


Figure 1. a) Schematic illustration for the preparation of Co-based catalysts with N-doped carbon layers enwrapping. TEM images of the as synthesized b) Co-MOFs and c) Co-MOFs@PDA-800. d) HRTEM image of Co-MOFs@PDA-800 showing Co NPs tightly wrapped by the well-developed graphitic layers. e) Dark-field TEM image of Co-MOFs@PDA-800 and examination of the corresponding elemental mappings of C, Co, and N.

understanding structure–function relationship through combining first-principle simulations.^[34–38]

In this study, a novel and facile surface engineering strategy has been demonstrated for the selective synthesis of Co-coordinated N-doped carbonaceous catalyst (Co–N–C) with favorable ORR electrocatalytic activity via surface polydopamine (PDA) coating layer-assisted pyrolysis approach. In this strategy, PDA, a well-known biopolymer which can easily adhere to the surface of virtually all kinds of solid materials regardless of their chemical nature, was employed as an ecofriendly nitrogen source in other works.^[24,39] The fabrication process is schematically depicted in **Figure 1a**. In brief, Co–MOFs nanosheets were synthesized from a mixed solution of $\text{Co}(\text{NO}_3)_2 \cdot 6\text{H}_2\text{O}$ and *p*-phthalic acid via a ultrasonication method. After adding dopamine (DA) in Co–MOFs nanosheets suspension, PDA would be self-polymerized at the surface of Co–MOFs nanosheets to

form a PDA coating layer (Co–MOFs@PDA). Finally, the Co–MOFs@PDA was subjected to a pyrolysis process at high temperature under N_2 atmosphere.

The ultrathin morphology of the as-synthesized Co–MOFs nanosheets can be clearly revealed by transmission electron microscopy (TEM) and field emission scanning electron microscope (FESEM) images (**Figure 1b**; **Figure S1**, Supporting Information). The spontaneously curling up of the Co–MOFs nanosheets edges suggest their outstanding flexibility (marked by the black arrow in **Figure 1b**). A typical Tyndall light scattering effect under laser irradiation was observed, indicating the stable colloid behavior of Co–MOFs nanosheets (inset of **Figure 1b**). After a pyrolysis process at 800 °C for 2 h under N_2 flow, the Co–MOFs without surface PDA coating layer was collapsed, and the crystallized Co phase prevailed, as confirmed by the appearance of large scale Co nanoparticles (NPs) (**Figure S2**, Supporting Information). However, under the same pyrolysis condition, the Co–MOFs with surface PDA coating layer derived Co–MOFs@PDA-*n* (*n* indicates the pyrolysis temperature (°C), *n* = 700, 800, and 900) samples retain the nanosheets morphology (**Figure 1c**; **Figure S3**, Supporting Information).

TEM image as shown in **Figure 1c** indicates that the Co–MOFs@PDA-800 consisting of flake-like structure nanosheets embedded with well-dispersed Co NPs were successfully synthesized after a pyrolysis process at 800 °C for 2 h under N_2 flow. The average particle size of Co NPs embedded in Co–MOFs@PDA-800 sample is ≈ 50 nm. It was noteworthy that the uniform deposition of PDA layer on the surface of Co–MOFs was able to offer sufficient confinement to suppress the Co metal particles from further irreversible fusion and aggregation at high temperature, resulting in the well dispersion of Co NPs after pyrolysis, while the PDA-free Co–MOFs resulted in the structure collapsed and formed self-aggregated uncontrollable large Co NPs under the same pyrolysis process due to the lack of the protection of the surface PDA coating layer. High-resolution TEM (HRTEM) image of Co–MOFs@PDA-800 clearly shows that the Co NPs are encapsulated by graphitic carbon layers (≈ 8 nm) with crystal lattice spacing of 3.4 Å corresponding to the (002) plane (**Figure 1d**), which should be attributed to the carbon graphitization under the catalytic behavior of Co NPs at high temperature.^[40] This result can also be confirmed by X-ray diffraction (XRD) results (**Figure 2a**). Elemental mapping images of Co–MOFs@PDA-800 indicate that the Co and N are homogeneously dispersed throughout the entire carbon framework (**Figure 1e**), resulting from the decomposition of Co–MOF and surface PDA coating layer precursors. The mass fraction

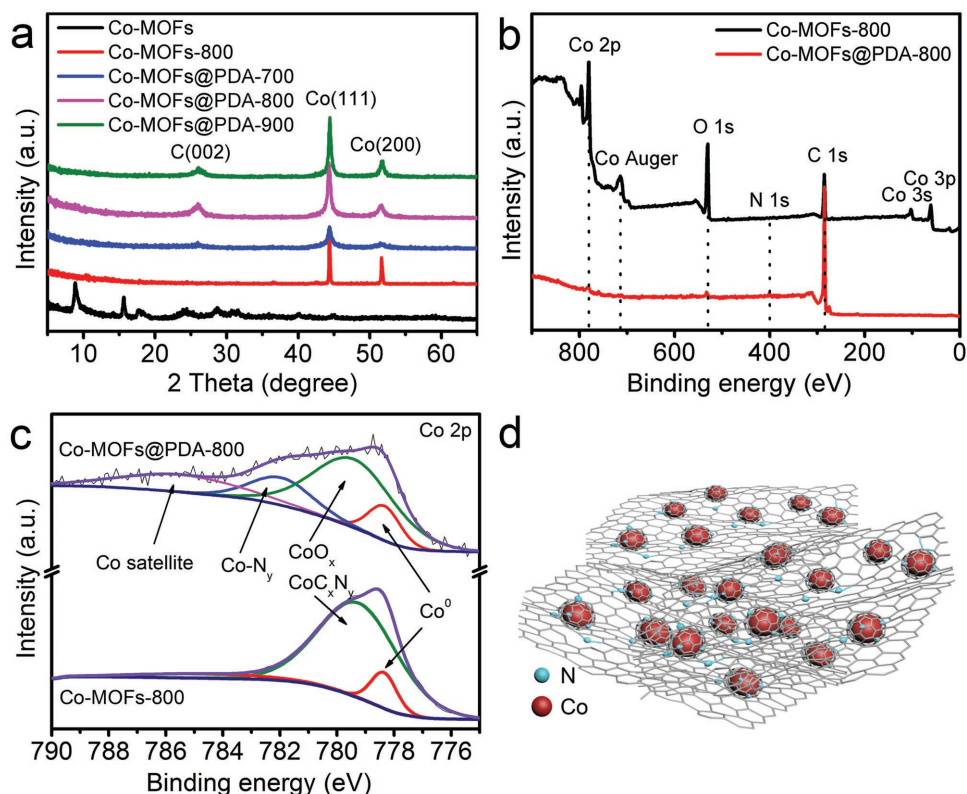


Figure 2. a) XRD of the as-synthesized Co-MOFs and their derived materials obtained at different pyrolysis temperatures. Comparison of the b) XPS survey spectra and c) high-resolution Co 2p XPS spectra of Co-MOFs-800 and Co-MOFs@PDA-800. d) The proposed structural model of Co-MOFs@PDA-800 hybrid.

of total Co loading in Co-MOFs@PDA-800 was ≈ 33.8 wt%, as confirmed by the thermogravimetric analysis (TGA) (Figure S4, Supporting Information).

The XRD patterns shown in Figure 2a investigated the compositions of Co-MOFs and their derived materials. XRD results reveal that the original peaks of Co-MOFs were disappeared and presented a series of new reflection peaks after the pyrolysis process. The XRD pattern of the Co-MOFs-800 derived from the PDA-free Co-MOFs exhibited two peaks at around 44° and 51° , which could be assigned to the (111) and (200) diffractions of metallic Co (JCPDS 01-1255), respectively. By contrast, the XRD pattern of Co-MOFs@PDA derived materials not only exhibit the two peaks of metallic Co, but also clearly show the peak located at around 26° corresponding to the (002) plane of graphitic carbon. This result suggests that the surface PDA coating layer provided abundant carbon precursor for the formation of graphitized carbon. It is well known that the Co components could catalyze the graphitization of carbon during pyrolysis in the formation of reduced metallic Co at $\geq 700^\circ\text{C}$,^[9,41] and the carbon graphitization can be beneficial to enhance the electronic conductivity and corrosion resistance in electrocatalysis.^[23] The Co induced formation of graphitized carbon is further supported by the Raman spectrum. There are two dominant peaks corresponding to D band at around 1340 cm^{-1} and G band at around 1590 cm^{-1} in the Raman spectra (Figure S5, Supporting Information).

To further study the surface chemical composition and binding energy (BE) of the Co-MOFs@PDA derived materials, the SRXPS analyses were performed (Figure 2b,c; Figures S6–S8, Supporting Information), and the signals of all X-ray photoelectron spectroscopy (XPS) data were fitted using a Voigt Gauss–Lorentz line shape GL(30). The XPS survey spectrum of Co-MOFs-800 clearly shows the sharp O and Co peaks (Figure 2b), indicating that the abundant Co NPs were exposed and oxidized. On the contrary, the XPS survey spectrum of Co-MOFs@PDA-800 revealed the sharp C peak and inconspicuous N peak, weakened O and Co peaks, which was benefited from the surface PDA coating layer providing C and N source, and in turn protecting the Co NPs from oxidation. The high-resolution Co 2p XPS spectrum of Co-MOFs-800 can be deconvoluted into two peaks (Figure 2c), corresponding to metallic Co (BE: 778.4 eV , full width at half-maximum, FWHM: 1.058 eV) and CoO_x or CoC_xN_y (BE: 779.7 eV , FWHM: 3.268 eV).^[11,30] However, the high-resolution Co 2p XPS spectrum of Co-MOFs@PDA-800 can be deconvoluted into four peaks, corresponding to metallic Co (BE: 778.4 eV , FWHM: 1.316 eV), CoO_x or CoC_xN_y (BE: 779.7 eV , FWHM: 3.360 eV), Co-N_y (BE: 782.1 eV , FWHM: 2.526 eV), and Co^{2+} shakeup satellite peak ($\approx 785.9\text{ eV}$).^[11,30] The fitting curves suggested the formation of Co–N bond in Co-MOFs@PDA-800, which has been identified as one of the most efficient active sites for the ORR.^[23] For comparison of the high-resolution Co 2p XPS spectra, the proportion of Co–N_y species decreased significantly with the increasing of

the pyrolysis temperature from 700 to 900 °C, indicating the breaking of some Co–N coordination bonds. The deconvoluted two peaks of high-resolution C 1s XPS spectrum of Co-MOFs@PDA-800 display two types of contributions for carbon species (Figure S6a, Supporting Information). The peak at 284.6 eV (FWHM: 1.422 eV) can be assigned to graphitic sp² carbon phase (C–C bond),^[41] and the other peak at 285.4 eV (FWHM: 2.823 eV) is originated from the sp² hybridized carbon containing nitrogen atoms (C–N bond).^[42] Furthermore, the high-resolution XPS spectrum for N 1s was divided into three types of N species (Figure S6b, Supporting Information), which can be assigned to pyridinic N and Co–N (BE: 398.2 eV, FWHM: 2.506 eV), pyrrolic N (BE: 400.5 eV, FWHM: 1.709 eV), and graphitic N (BE: 401.4 eV, FWHM: 2.914 eV), respectively.^[26,43] Due to the lone-pair electrons, both the two kinds of the pyridinic N and pyrrolic N can serve as metal coordination sites.^[14,23] Moreover, the proportion of the pyridinic N decreased significantly with the pyrolysis temperature increasing from 700 to 900 °C, demonstrating that some Co–N coordination bonds were broken.^[12] In our synthesis, the in situ formed N-doped graphitic carbon materials cannot only provide strong support for the N-coordinated Co NPs, but also regulate the surface electron structure (Figure 2d).

To give an in-depth identification of the local coordination structure of Co NPs and electronic structure in the products, soft X-ray absorption near-edge structure (XANES) measurements were employed. As shown in Figure 3a, all the C K-edge XANES spectra display two main regions assigned to the π* region of

graphitic C=C at ≈285 eV and the doublet σ* resonance peak of C–C at ≈292 eV, respectively.^[44] Compared to Co-MOFs-800, Co-MOFs@PDA-800 shows a significant decrease of C K-edge peak intensity at ≈288.2 and ≈290 eV which are typically attributed to C=O and carboxylic (–COOH), respectively.^[45] This result suggested the possible formation of interfacial Co–O–C in Co-MOFs-800 due to easy oxidation without carbon enveloping. Besides, the peak at ≈290 eV for Co-MOFs-800 and the peak at ≈288.2 eV for Co-MOFs@PDA-800 decreased severally when the pyrolysis temperature increased from 800 to 900 °C, which were caused by the Co catalyzed graphitization and thus reduced their defect levels. The N K-edge XANES spectra of Co-MOFs@PDA-*n* samples exhibited the second-order photon excited Co L2 peak at ≈397 eV, π* peaks at ≈400 eV (≈399 eV for pyridinic; ≈400 eV for pyrrolic; ≈401 eV for graphitic) and σ* peak at ≈406 eV (Figure 3b).^[46] The weakening of the N K-edge XANES spectra with the increasing of the pyrolysis temperature from 700 to 900 °C could be attributed to the breaking of some Co–N coordination bonds. This result indicates the formation of covalent interfacial Co–N–C bonds in the Co-MOFs@PDA derived hybrid materials. As shown in Figure 3c, the Co L-edge XANES spectrum of the Co-MOFs-800 showed obviously enhanced absorption compared to that of Co-MOFs@PDA-800, suggesting surface oxidation of the Co NPs,^[47,48] consistent with the XPS analyses. The ratio of high-energy/low-energy peaks in Co L3 edge decreased markedly for Co-MOFs@PDA-800 compared to that of Co-MOFs-800, also suggesting the less surface oxidation of Co NPs.^[49]

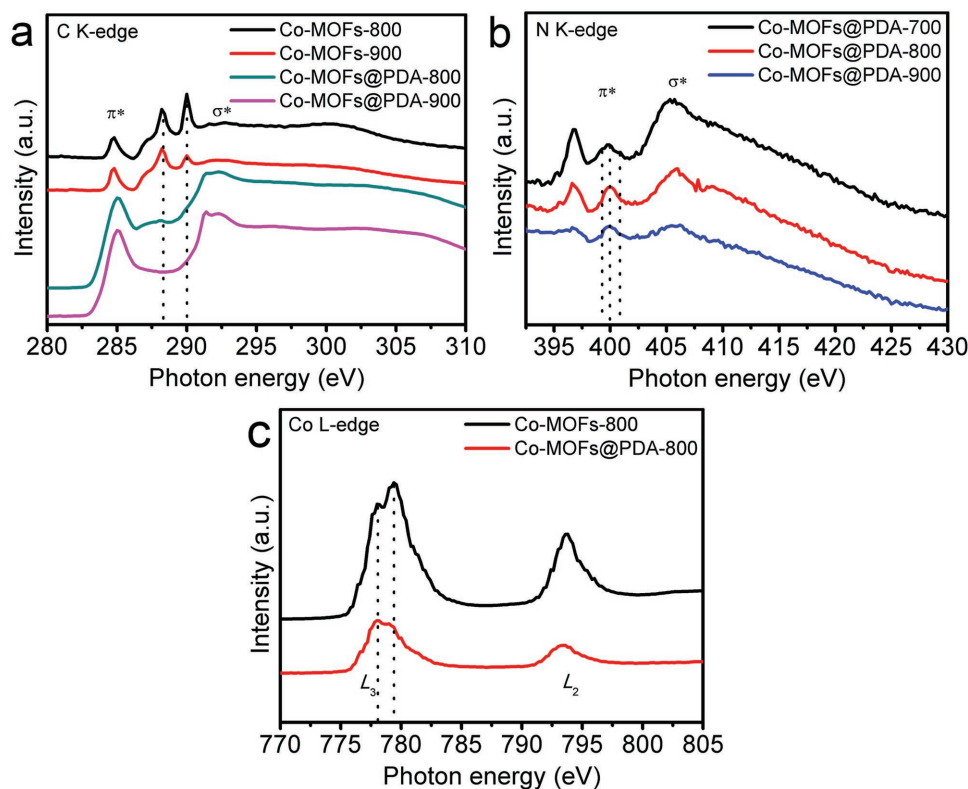


Figure 3. a) C K-edge XANES of Co-MOFs-800, Co-MOFs-900, Co-MOFs@PDA-800, and Co-MOFs@PDA-900. b) N K-edge XANES of Co-MOFs@PDA-*n*. c) Co L-edge XANES of Co-MOFs-800 and Co-MOFs@PDA-800.

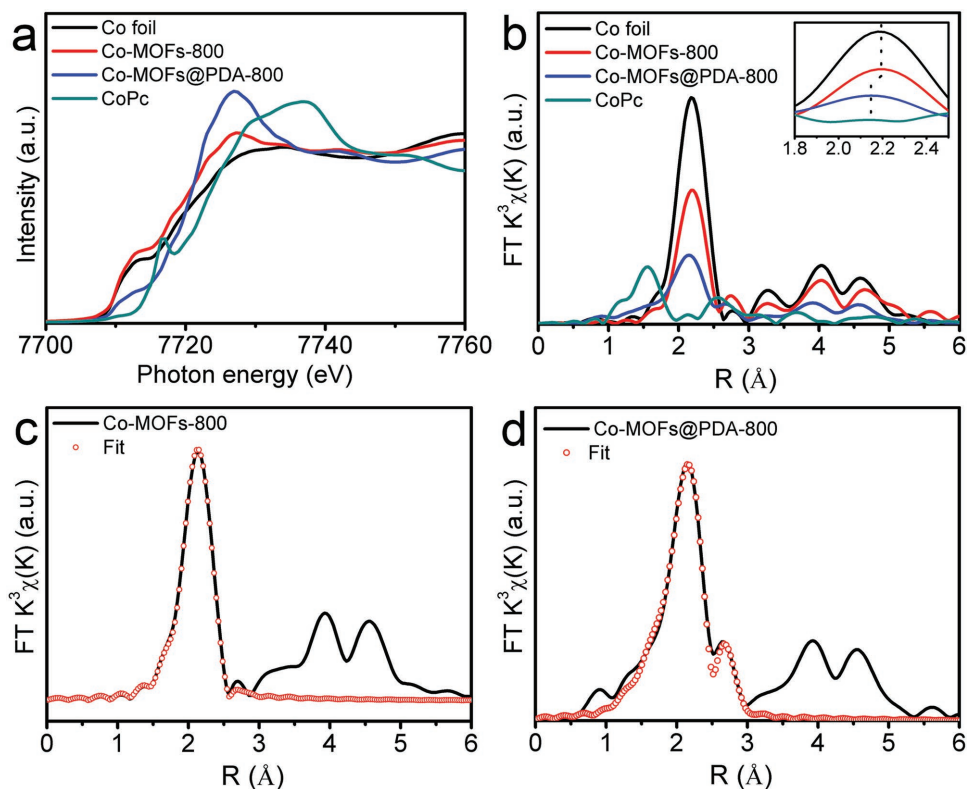


Figure 4. a) Normalized Co K-edge XANES spectra of Co-MOFs@PDA-800 as well as the Co foil and Cobalt phthalocyanine (CoPc) reference samples. b) The corresponding k^3 -weighted $\chi(k)$ -function of the Co K-edge EXAFS spectra. c,d) The FT k^3 -weighted spectra in R space of the experimental and first-shell fitted for Co-MOFs-800 and Co-MOFs@PDA-800, respectively.

To further study the atomic structure of Co species in catalysts, the Co K-edge of Co-MOFs-800 and Co-MOFs@PDA-800 samples were investigated using X-ray absorption fine structure (XAFS) analyses. As shown in **Figure 4a**, the overall spectrum of Co K-edge XANES of Co-MOFs@PDA-800 can be clearly distinguished from the reference Co foil and cobalt phthalocyanine (CoPc). The coordination environments of the Co atoms in Co-MOFs-800 and Co-MOFs@PDA-800 were further corroborated using Fourier transformed (FT) k^3 -weighted extended X-ray absorption fine structure (EXAFS) spectrum at the Co K-edge (**Figure 4b**). The EXAFS spectra show the similar curves to that of the reference Co foil, indicating that the Co–Co bonding could be the main contributor in the as-obtained Co-MOFs-800 and Co-MOFs@PDA-800. On the other hand, compared with Co foil and Co-MOFs-800, the EXAFS spectrum of Co-MOFs@PDA-800 shows a slight shifts to low-R, as shown in the inset of **Figure 4b**, indicating that the Co atoms have been embedded on carbon network, consistent with TEM results. Similar phenomenon has been reported elsewhere.^[50] In addition, the Co-MOFs@PDA-800 exhibits decreased Co–Co coordination number and bond length compared with the reference Co foil and Co-MOFs-800, implying surface distortion and atomic environmental change of Co NPs. Fitting analyses were carried out for the first coordination shell for Co-MOFs-800, Co-MOFs@PDA-800 and Co foil (**Figure 4c,d**; **Figure S9**, Supporting Information). The best-fitting parameters (**Table 1**) reveal the coexistence of Co–N and Co–Co bonds, further corroborating the abovementioned TEM, XPS, and soft XANES results. Recent

reports indicated that such structure with N-doped carbon layers enwrapped metal NPs delivers efficient ORR activities, in which metal NPs boost the activity of Metal–N_x and C–N_x due to interfacial charge transfer.^[51–53]

The ORR electrocatalytic activities of the as-prepared Co-MOFs derived hybrid materials were assessed in KOH (0.1 M) solution via cyclic voltammetry (CV) and linear sweep voltammetry (LSV) methods on rotating disk electrode (RDE) or rotating ring disk electrode (RRDE). As shown in **Figure 5a**, there was no obvious featured peak for Co-MOFs@PDA-800 in the N₂-saturated KOH solution, while a well-defined cathodic peak toward ORR was obviously enhanced in O₂-saturated KOH solution, indicating a distinct ORR activity of this sample. **Figure 5b** shows the comparison of LSV curves of different samples recorded on the RDE at a scan rate of 10 mV s^{−1} with a rotation speed of 1600 rpm. It can be seen that the Co-MOFs@PDA-800 exhibits a superior diffusion-limited

Table 1. EXAFS data fitting results from Co-edge of samples. *N*, coordination number; *R*, bond distance; σ^2 , Debye–Waller factor value. S_0^2 was fixed to 0.86 as determined from Co foil fitting.

Sample	Path	<i>N</i>	<i>R</i> [Å]	σ^2 [10 ^{−3} Å ²]
Co foil	Co–Co	12.0	2.496	6.00
Co-MOFs-800	Co–Co	11.2	2.496	6.62
Co-MOFs@PDA-800	Co–Co	5.2	2.518	8.23
	Co–N	3.3	2.100	7.37

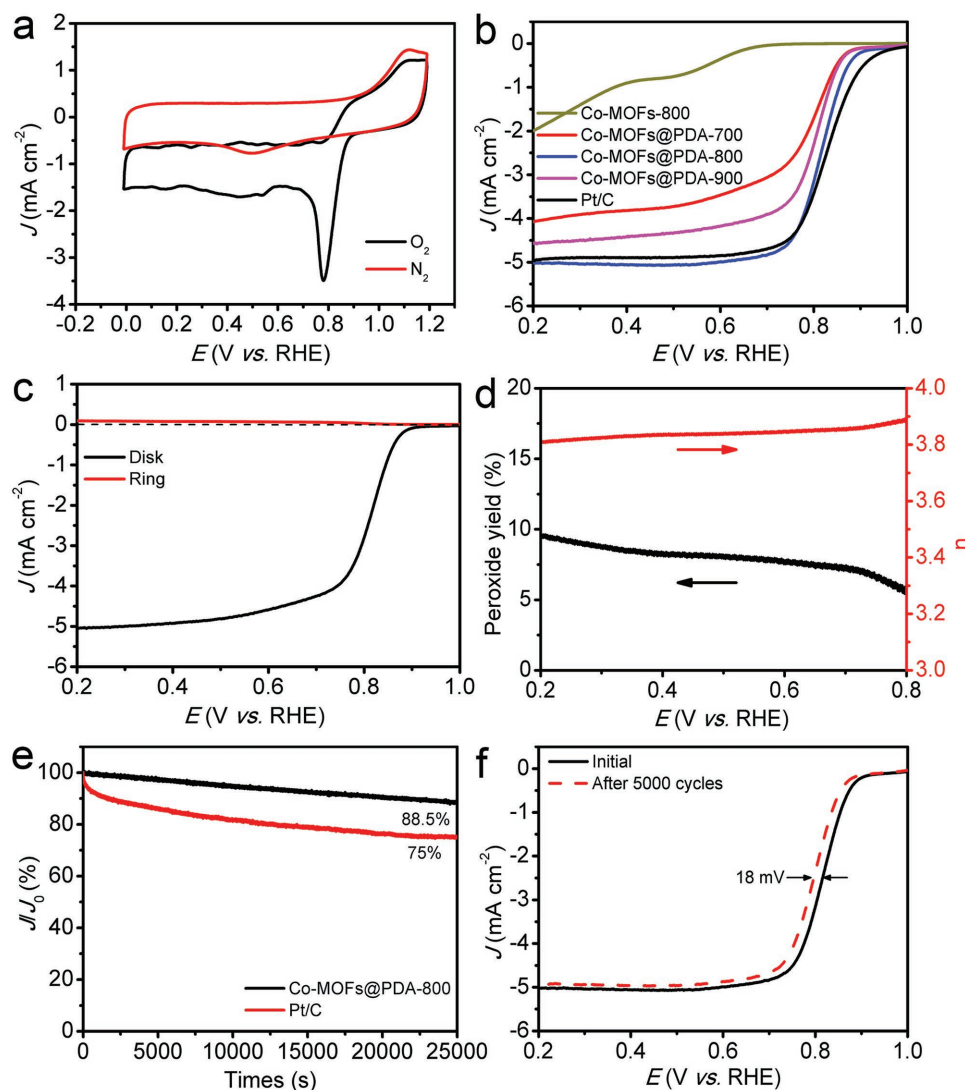


Figure 5. a) CV curves of Co-MOFs@PDA-800 in N_2 -saturated and O_2 -saturated 0.1 M KOH. b) LSV curves for different samples in O_2 -saturated 0.1 M KOH solution at a rotation rate of 1600 rpm. c) RRDE voltammograms and d) peroxide yield (black) with regard to the total oxygen reduction products and the electron-transfer number (n) (red) of Co-MOFs@PDA-800 in O_2 -saturated 0.1 M KOH at 1600 rpm. e) Current-time chronoamperometric responses of Co-MOFs@PDA-800 and 20% Pt/C at 0.4 V in O_2 -saturated 0.1 M KOH solution. f) Endurance test of Co-MOFs@PDA-800 catalyst for 5000 CV cycles in O_2 -saturated 0.1 M KOH.

current density (J_L) (5.1 mA cm^{-2}) to the performances of Co-MOFs-800, Co-MOFs@PDA-700, and Co-MOFs@PDA-900. Moreover, the Co-MOFs@PDA-800 catalyst posed a negative onset potential (0.923 V vs reversible hydrogen electrode, RHE) than that of Pt/C (0.976 V vs RHE), and the value of the half-wave potential of the Co-MOFs@PDA-800 (0.816 V vs RHE) was only 14 mV less than that of Pt/C (0.830 V vs RHE), and exhibited a comparable ORR performance to other reference catalysts (Table S1, Supporting Information), suggesting a satisfied electrocatalytic activity of Co-MOFs@PDA-800 for ORR.

RDE measurements were carried out with different rotation speeds at a scan rate of 10 mV s^{-1} in O_2 -saturated 0.1 M KOH solution to investigate the reaction kinetics of the as-prepared samples. The LSV curves of Co-MOFs@PDA-800 were measured via the RDE show that the onset potential remains

constant under various rotating speeds (Figure S10a, Supporting Information), while the J_L increased with the rotating speeds increasing from 225 to 2500 rpm owing to the improved mass transport at higher speeds.^[54] The corresponding Koutecký–Levich (K–L) plots (J^{-1} vs $\omega^{-1/2}$) for Co-MOFs@PDA-800 at different potentials from 0.4 to 0.6 V versus RHE show the fairly well linearity and near coincidence (Figure S10b, Supporting Information), suggesting first-order reaction kinetics with respect to the dissolved oxygen concentration.^[14] For comparison, the LSV curves and K–L plots of the other samples were also measured (Figures S11–S13, Supporting Information).

To further investigate the ORR kinetics of Co-MOFs@PDA-800, RRDE measurement was performed (Figure 5c). The percentage of the formed peroxide species during the ORR process and the electron transfer number (n) curves were calculated from RRDE data (Figure 5d). The peroxide yield (%) of

Co-MOFs@PDA-800 is below 10% and the average n calculated from the curve is ≈ 3.85 within 0.2–0.8 V versus RHE, indicating a nearly four-electron transfer pathway for ORR. Moreover, $i-t$ curves of Co-MOFs@PDA-800 and Pt/C were evaluated. Co-MOFs@PDA-800 shows only a slight anodic current attenuation of 11.5% within 25 000 s, whereas Pt/C displays larger current attenuation of 25% (Figure 5e). After 5000 CV cycles, the half-wave potential for Co-MOFs@PDA-800 exhibited a small negative shift of about 18 mV (Figure 5f). This result demonstrates that the Co-MOFs@PDA-800 electrode possesses better catalytic stability than the commercial 20 wt% Pt/C catalyst for ORR in 0.1 M KOH medium.

In summary, we developed a facile approach to synthesize a well-defined cobalt electrocatalyst with N-doped carbon enwrapping via surface engineering in catalysts preparation and active sites regulations. The surface atomic structure was clearly identified by X-ray characterizations. The electrocatalytic measurements showed that the resulting Co-MOFs@PDA-800 catalyst displayed comparable ORR catalytic activities and better long-term stability compared to the commercial 20 wt% Pt/C catalyst, suggesting the potential of their practical applications. The outstanding electrocatalytic performances of the Co-MOFs@PDA-800 for ORR were associated with engineered surface coating and active site regulations. The present results can provide an efficient way to characterize the atomic structure of hybrid catalyst, and will also significantly broaden the synthesis strategies for developing novel MOFs-derived nonprecious electrocatalysts with controllable morphology and functionality for future applications.

Experimental Section

Materials: All chemicals were purchased and used directly as received. Cobalt nitrate hexahydrate ($\text{Co}(\text{NO}_3)_2 \cdot 6\text{H}_2\text{O}$, 98.5%), ethanol ($\text{C}_2\text{H}_5\text{OH}$, >99.7%), *p*-phthalic acid (PPA, 99%), *N,N*-dimethylformamide (DMF, 99.5%), and potassium hydroxide (KOH, >85%) was bought from Sinopharm Chemical Reagent. Nafion solution (5 wt%) and dopamine hydrochloride (DA, 98%) were purchased from Alfa Aesar. Triethylamine (TEA), poly(ethylene oxide)-poly(propylene oxide)-poly(ethylene oxide) (P123), and Trizma base (Tris, 99.9%) were bought from Sigma-Aldrich Reagent. The deionized water (DIW) was used in all the experiments.

Synthesis of Co-MOFs Nanosheets: The synthesis of Co-MOFs nanosheets was based on a previous procedure with some modifications.^[55] In brief, PPA (0.75 mmol) was dissolved into the mixed solution contained DMF (32 mL), ethanol (2 mL), and DIW (2 mL) under ultrasonication. Subsequently, $\text{Co}(\text{NO}_3)_2 \cdot 6\text{H}_2\text{O}$ (0.75 mmol) was added under stirring until the solution became clear. Then, TEA (0.8 mL) was quickly injected into the solution. The solution was magnetic stirred continuously for 5 min to obtain a uniform colloidal suspension. Afterwards, the solution was continuously ultrasonicated for 60 min (40 kHz) under airtight conditions at room temperature (RT). Finally, the products were collected via centrifugation at 7000 rpm for 10 min and washed with ethanol and DIW for several times followed by a freeze-drying process.

Synthesis of Co-MOFs@PDA: The as-prepared Co-MOFs powder (100 mg), P123 (75 mg), and Tris (160 mg) were initially dispersed in DIW (100 mL) and sonicated for 30 min to form a homogenous solution, then, continuously magnetic stirred at RT for 2 h. Subsequently, 20 mL solution contained DA (100 mg) was added into above dispersion, and continuously magnetic stirred at RT for 24 h to form Co-MOFs@PDA. The products were collected by centrifugation at 7000 rpm for 10 min and washed by DIW for 5 times followed by a freeze-drying process.

Synthesis of Co-MOFs@PDA Derived Catalysts: The as-synthesized Co-MOFs@PDA powder was thermally decomposed at the desired temperature (700, 800, and 900 °C) for 2 h under flowing N_2 atmosphere with a heating rate of 3 °C min^{-1} and cooled to RT naturally, the obtain resulting product is denoted as Co-MOFs@PDA- n (n indicates the pyrolysis temperature (°C), $n = 700, 800, \text{ and } 900$). For a comparison study, PDA-free Co-MOFs-800 was prepared as a control sample via the same pyrolysis procedure at 800 °C for 2 h.

Characterization: Powder XRD studies of samples were carried out on a Philips X'Pert Pro Super X-ray diffractometer with $\text{Cu-K}\alpha$ radiation ($\lambda = 1.54178 \text{ \AA}$). The morphological studies of the products were characterized by using JEOL JSM 6700F FESEM and JEOL JEM 2010 TEM equipped with an energy-dispersive X-ray spectrometer (Oxford Instruments) for elemental mapping. Raman spectra were collected on an XploRA Raman spectrometer with 532 nm wavelength incident laser light. The TGA was performed on a TGA Q5000 (TA Instruments) in air flow from RT to 800 at 10 °C min^{-1} . XPS measurements were undertaken at the Photoemission Endstation connected at the BL10B beamline equipped a VG-Scientia R3000 electron-energy analyzer with an Al $\text{K}\alpha = 1482.3 \text{ eV}$ source in National Synchrotron Radiation Laboratory (NSRL) in Hefei, China. The binding energies of XPS spectral range were calibrated for specimen charging effects using the C1s level at the energy of 284.6 eV as a reference.^[56] The Co K-edge XAFS spectra were carried at the 1W1B beamline station of the Beijing Synchrotron Radiation Facility (BSRF) and recorded in transmission mode using a Si(111) double-crystal monochromator. The C K-edge, N K-edge, and Co L-edge XANES spectra were recorded at BL12B- α beamline of NSRL. The acquired EXAFS data were processed according to the standard procedures using the ATHENA module implemented in the IFEFFIT software packages.^[57]

Electrochemical Test: All electrochemical measurements were performed using a three-electrode system on a CHI760E workstation (Shanghai Chenhua, China) and rotation control device (Pine Research Instrumentation) in 0.1 M KOH (pH = 13) electrolyte at RT. The working electrode was prepared by ultrasonically mixing 2 mg of the as-synthesized catalyst with the mixture of 480 μL ethanol and 20 μL 5 wt% Nafion solutions for 60 min to form a well dispersed catalyst ink. Next, 10 μL of the catalyst ink was carefully dropped onto the polished glassy carbon of 5 mm in diameter RDE or RRDE, followed by drying in air, leading to a desirable catalyst loading (with the mass loading of 0.204 mg cm^{-2}). The RDE coated with the catalyst ink was served as the working electrode, a platinum mesh electrode as the counter electrode, and Ag/AgCl double junction electrode as the reference electrode. For comparison, Pt/C (20 wt% platinum) with the similar mass loading was conducted on the same electrochemical tests.

The electrochemical potentials measured against the Ag/AgCl reference electrode were converted to the RHE scale via the Nernst equation^[21]

$$V \text{ vs RHE} = 0.0591 \times \text{pH} + 0.199(\text{Ag/AgCl in sat.KCl}) + V \text{ vs Ag/AgCl} \quad (1)$$

Before the measurement, a N_2 or O_2 flow was used through the electrolyte for 30 min to saturate it with N_2 or O_2 , and the catalyst was subjected to a number of CV cycles until a stable CV curve was obtained. The CV curves were obtained in N_2 or O_2 saturated 0.1 M KOH solution at a scan rate of 50 mV s^{-1} . RDE tests were measured by LSV from 1 V to 0.2 V versus RHE in O_2 -saturated 0.1 M KOH with a sweep rate of 10 mV s^{-1} at various rotating speeds from 225 to 2500 rpm. The ORR stability was carried out by a $i-t$ chronoamperometric measurement in O_2 -saturated 0.1 M KOH solution at a fixed potential of -0.40 V versus Ag/AgCl and the response current recorded against time up to 25 000 s in O_2 saturated 0.1 M KOH electrolyte at a rotating rate of 1600 rpm.

RRDE measurements were conducted by LSV from 1 to 0.2 V versus RHE at a scan rate of 5 mV s^{-1} at 1600 rpm, while the ring electrode was held at 1.3 V versus RHE. The electron-transfer number (n) and the yield of hydrogen peroxide (H_2O_2) released during ORR were calculated based on the following equations

$$n = 4 \times \frac{I_D}{I_D + I_R/N} \quad (2)$$

$$\text{H}_2\text{O}_2(\%) = 200 \times \frac{I_R/N}{I_D + I_R/N} \quad (3)$$

where I_D is the disk current, I_R is the ring current, and N represents the collection coefficient of the Pt ring ($N = 0.37$).

Supporting Information

Supporting Information is available from the Wiley Online Library or from the author.

Acknowledgements

Y.Z. and Y.L. contributed equally to this work. This work was financially supported by MOST (2017YFA0303500, 2014CB848900), NSFC (U1532112, 11375198, 11574280, 11605201), China Postdoctoral Science Foundation (BH2310000033), CAS Interdisciplinary Innovation Team and Key Laboratory of Advanced Energy Materials Chemistry (Ministry of Education) Nankai University. L.S. acknowledges the recruitment program of global experts, the CAS Hundred Talent Program. The authors thank the Shanghai synchrotron Radiation Facility (14W1, SSRF), the Beijing Synchrotron Radiation Facility (1W1B and soft-X-ray endstation, BSRF), the Hefei Synchrotron Radiation Facility (Photoemission, MCD, and Catalysis/Surface Science Endstations, NSRL), and the USTC Center for Micro and Nanoscale Research and Fabrication for helps in characterizations.

Conflict of Interest

The authors declare no conflict of interest.

Keywords

coating layers, electrocatalysts, oxygen reduction reaction, surface engineering, X-ray absorption spectroscopy

Received: June 19, 2017
Revised: October 21, 2017
Published online:

- [1] M. Yoon, R. Srirambalaji, K. Kim, *Chem. Rev.* **2011**, *112*, 1196.
[2] J. Pan, G. Liu, G. Q. M. Lu, H. M. Cheng, *Angew. Chem., Int. Ed.* **2011**, *50*, 2133.
[3] H. Wei, X. Liu, A. Wang, L. Zhang, B. Qiao, X. Yang, Y. Huang, S. Miao, J. Liu, T. Zhang, *Nat. Commun.* **2014**, *5*, 5634.
[4] J. Kibsgaard, Z. Chen, B. N. Reinecke, T. F. Jaramillo, *Nat. Mater.* **2012**, *11*, 963.
[5] D.-W. Wang, D. Su, *Energy Environ. Sci.* **2014**, *7*, 576.
[6] Y. Liang, Y. Li, H. Wang, J. Zhou, J. Wang, T. Regier, H. Dai, *Nat. Mater.* **2011**, *10*, 780.
[7] G. Zhang, B. Y. Xia, X. Wang, *Adv. Mater.* **2014**, *26*, 2408.
[8] H. Yin, C. Zhang, F. Liu, Y. Hou, *Adv. Funct. Mater.* **2014**, *24*, 2930.
[9] V. Armel, S. Hindocha, F. Salles, S. Bennett, D. Jones, F. Jaouen, *J. Am. Chem. Soc.* **2017**, *139*, 453.
[10] W. Xia, A. Mahmood, R. Zou, Q. Xu, *Energy Environ. Sci.* **2015**, *8*, 1837.
[11] Z. Li, M. Shao, L. Zhou, R. Zhang, C. Zhang, M. Wei, D. G. Evans, X. Duan, *Adv. Mater.* **2016**, *28*, 2337.
[12] P. Yin, T. Yao, Y. Wu, L. Zheng, Y. Lin, W. Liu, H. Ju, J. Zhu, X. Hong, Z. Deng, G. Zhou, S. Wei, Y. Li, *Angew. Chem., Int. Ed.* **2016**, *55*, 10800.
[13] P. Zhang, F. Sun, Z. Xiang, Z. Shen, J. Yun, D. Cao, *Energy Environ. Sci.* **2014**, *7*, 442.
[14] L. Lin, Q. Zhu, A.-W. Xu, *J. Am. Chem. Soc.* **2014**, *136*, 11027.
[15] Y. Zhao, K. Watanabe, K. Hashimoto, *J. Am. Chem. Soc.* **2012**, *134*, 19528.
[16] J. Zhu, M. Xiao, Y. Zhang, Z. Jin, Z. Peng, C. Liu, S. Chen, J. Ge, W. Xing, *ACS Catal.* **2016**, *6*, 6335.
[17] C. You, X. Jiang, L. Han, X. Wang, Q. Lin, Y. Hua, C. Wang, X. Liu, S. Liao, *J. Mater. Chem. A* **2017**, *5*, 1742.
[18] G. Fazio, L. Ferrighi, C. D. Valentin, *J. Catal.* **2016**, *318*, 203.
[19] Z. Yang, J. Wu, X. Zheng, Z. Wang, R. Yang, *J. Power Sources* **2015**, *277*, 161.
[20] T. Sun, Q. Wu, O. Zhuo, Y. Jiang, Y. Bu, L. Yang, X. Wang, Z. Hu, *Nanoscale* **2016**, *8*, 8480.
[21] Z. Zhang, X. Gao, M. Dou, J. Ji, F. Wang, *J. Mater. Chem. A* **2017**, *5*, 1526.
[22] G. Wu, K. L. More, C. M. Johnston, P. Zelenay, *Science* **2011**, *332*, 443.
[23] Y.-Z. Chen, C. Wang, Z.-Y. Wu, Y. Xiong, Q. Xu, S.-H. Yu, H.-L. Jiang, *Adv. Mater.* **2015**, *27*, 5010.
[24] J. Xi, Y. Xia, Y. Xu, J. Xiao, S. Wang, *Chem. Commun.* **2015**, *51*, 10479.
[25] H. T. Chung, J. H. Won, P. Zelenay, *Nat. Commun.* **2013**, *4*, 1922.
[26] Q. L. Zhu, W. Xia, T. Akita, R. Zou, Q. Xu, *Adv. Mater.* **2016**, *28*, 6391.
[27] J. Liang, Y. Jiao, M. Jaroniec, S. Z. Qiao, *Angew. Chem., Int. Ed.* **2012**, *51*, 11496.
[28] K. Gong, F. Du, Z. Xia, M. Durstock, L. Dai, *Science* **2009**, *323*, 760.
[29] W. Zhang, Z.-Y. Wu, H.-L. Jiang, S.-H. Yu, *J. Am. Chem. Soc.* **2014**, *136*, 14385.
[30] S. H. Ahn, M. J. Klein, A. Manthiram, *Adv. Energy Mater.* **2016**, *7*, 1601979.
[31] Y. Hou, T. Huang, Z. Wen, S. Mao, S. Cui, J. Chen, *Adv. Energy Mater.* **2014**, *4*, 1400337.
[32] B. Y. Xia, Y. Yan, N. Li, H. B. Wu, X. W. D. Lou, X. Wang, *Nat. Energy* **2016**, *1*, 15006.
[33] P. Yin, T. Yao, Y. Wu, L. Zheng, Y. Lin, W. Liu, H. Ju, J. Zhu, X. Hong, Z. Deng, *Angew. Chem., Int. Ed.* **2016**, *55*, 10800.
[34] S.-C. Qi, L. Zhang, H. Einaga, S. Kudo, K. Norinaga, J.-i. Hayashi, *J. Mater. Chem. A* **2017**, *5*, 3948.
[35] Y. Li, S. Chen, R. Long, H. Ju, Z. Wang, X. Yu, F. Gao, Z. Cai, C. Wang, Q. Xu, *Nano Energy* **2017**, *34*, 306.
[36] T. Xiang, Q. Fang, H. Xie, C. Wu, C. Wang, Y. Zhou, D. Liu, S. Chen, A. Khalil, S. Tao, *Nanoscale* **2017**, *9*, 6975.
[37] H. Li, S. Chen, X. Jia, B. Xu, H. Lin, H. Yang, L. Song, X. Wang, *Nat. Commun.* **2017**, *8*, 15377.
[38] Q. Liu, X. Li, Z. Xiao, Y. Zhou, H. Chen, A. Khalil, T. Xiang, J. Xu, W. Chu, X. Wu, *Adv. Mater.* **2015**, *27*, 4837.
[39] H. P. Cong, P. Wang, M. Gong, S. H. Yu, *Nano Energy* **2014**, *3*, 55.
[40] J. Hoekstra, A. M. Beale, F. Soulimani, M. Versluijs-Helder, J. W. Geus, L. W. Jenneskens, *J. Phys. Chem. C* **2015**, *119*, 10653.
[41] S. Gadipelli, T. Zhao, S. A. Shevlin, Z. Guo, *Energy Environ. Sci.* **2016**, *9*, 1661.
[42] C. Y. Su, H. Cheng, W. Li, Z. Q. Liu, N. Li, Z. Hou, F. Q. Bai, H. X. Zhang, T. Y. Ma, *Adv. Energy Mater.* **2017**, *7*, 1602420.
[43] H. Fei, J. Dong, M. J. Arellano-Jiménez, G. Ye, N. D. Kim, E. L. G. Samuel, Z. Peng, Z. Zhu, F. Qin, J. Bao, *Nat. Commun.* **2015**, *6*, 8668.
[44] P. Chen, T. Zhou, L. Xing, K. Xu, Y. Tong, H. Xie, L. Zhang, W. Yan, W. Chu, C. Wu, *Angew. Chem., Int. Ed.* **2017**, *56*, 610.

- [45] D. Wang, J. Yang, X. Li, D. Geng, R. Li, M. Cai, T.-K. Sham, X. Sun, *Energy Environ. Sci.* **2013**, *6*, 2900.
- [46] Y. Liang, H. Wang, J. Zhou, Y. Li, J. Wang, T. Regier, H. Dai, *J. Am. Chem. Soc.* **2012**, *134*, 3517.
- [47] Y. Liang, H. Wang, P. Diao, W. Chang, G. Hong, Y. Li, M. Gong, L. Xie, J. Zhou, J. Wang, *J. Am. Chem. Soc.* **2012**, *134*, 15849.
- [48] M. Gong, W. Zhou, M.-C. Tsai, J. Zhou, M. Guan, M.-C. Lin, B. Zhang, Y. Hu, D.-Y. Wang, J. Yang, S. J. Pennycook, B.-J. Hwang, H. Dai, *Nat. Commun.* **2014**, *5*, 4695.
- [49] A. Tuxen, S. Carenco, M. Chintapalli, C.-H. Chuang, C. Escudero, E. Pach, P. Jiang, F. Borondics, B. Beberwyck, A. P. Alivisatos, *J. Am. Chem. Soc.* **2013**, *135*, 2273.
- [50] X. Li, W. Bi, L. Zhang, S. Tao, W. Chu, Q. Zhang, Y. Luo, C. Wu, Y. Xie, *Adv. Mater.* **2016**, *28*, 2427.
- [51] W.-J. Jiang, L. Gu, L. Li, Y. Zhang, X. Zhang, L.-J. Zhang, J.-Q. Wang, J.-S. Hu, Z. Wei, L.-J. Wan, *J. Am. Chem. Soc.* **2016**, *138*, 3570.
- [52] C. H. Choi, W. S. Choi, O. Kasian, A. K. Mechler, M. T. Sougrati, S. Brüller, K. Strickland, Q. Jia, S. Mukerjee, K. J. J. Mayrhofer, *Angew. Chem., Int. Ed.* **2017**, *129*, 8935.
- [53] L. Lu, Q. Hao, W. Lei, X. Xia, P. Liu, D. Sun, X. Wang, X. Yang, *Small* **2015**, *11*, 5833.
- [54] W. Ai, Z. Luo, J. Jiang, J. Zhu, Z. Du, Z. Fan, L. Xie, H. Zhang, W. Huang, T. Yu, *Adv. Mater.* **2014**, *26*, 6186.
- [55] S. Zhao, Y. Wang, J. Dong, C.-T. He, H. Yin, P. An, K. Zhao, X. Zhang, C. Gao, L. Zhang, J. Lv, J. Wang, J. Zhang, A. M. Khattak, N. A. Khan, Z. Wei, J. Zhang, S. Liu, H. Zhao, Z. Tang, *Nat. Energy* **2016**, *1*, 16184.
- [56] Y. Zhang, X. Dou, M. Yang, H. He, C. Jing, Z. Wu, *J. Hazard. Mater.* **2010**, *179*, 208.
- [57] G. Wu, W. Chen, X. Zheng, D. He, Y. Luo, X. Wang, J. Yang, Y. Wu, W. Yan, Z. Zhuang, X. Hong, Y. Li, *Nano Energy* **2017**, *38*, 167.